Journal of Alloys and Compounds 509 (2011) 1045–1049

Contents lists available at ScienceDirect

Journal of Alloys and Compounds

journal homepage: www.elsevier.com/locate/jallcom

Thermal conductivity of EB-PVD ZrO_2–4 mol% Y_2O_3 films using the laser flash method

Byung-Koog Jang[a,*], Yoshio Sakka[a], Norio Yamaguchi[b], Hideaki Matsubara[b], Hyung-Tae Kim[c]

[a] Nano Ceramics Center, National Institute for Materials Science, 1-2-1 Sengen, Tsukuba, Ibaraki 305-0047, Japan
[b] Japan Fine Ceramics Center, 2-4-1 Mutsuno, Atsuta-ku, Nagoya 456-8587, Japan
[c] Engineering Ceramic Center, Korea Institute of Ceramic Engineering and Technology, Icheon, Gyeonggi-do 467-843, Republic of Korea

ARTICLE INFO

Article history:
Received 2 August 2010
Received in revised form 16 August 2010
Accepted 26 August 2010
Available online 20 October 2010

Keywords:
Electron beam-physical vapor deposition
Zirconia
Laser flash method
Thermal conductivity

ABSTRACT

The variation in thermal conductivity and thermal diffusivity of ZrO_2–4 mol% Y_2O_3 coatings deposited onto Inconel substrates by EB-PVD is examined as a function of coating thickness using the laser flash method. The coatings are found to consist of columnar grains with a feather-like microstructure. The thermal conductivities of the coatings are calculated using two methods: the first involves separating the coating from the substrate and measuring the thermal diffusivity directly; the second uses thermal diffusion results from coatings still attached to the substrate and is based on the response function method. The results of both methods are in excellent agreement, and show that the thermal conductivities of the coatings increase with increasing coating thickness. The results also confirm that the double layer method can be used successfully to calculate the thermal conductivities of thin film coatings.

1. Introduction

Electron beam-physical vapor deposition (EB-PVD) is a widely used method for depositing thermal barrier coatings (TBCs) on superalloy substrates for high temperature applications such as in gas turbine engines [1–5]. Although the adhesion of these coatings to the superalloy substrates is of primary importance, the thermal conductivity of the coating is also one of the most critical properties in designing superior TBCs.

Typically TBCs have a porous structure, which means they have poor strength and are easily damaged [6,7]. In practice, therefore, it is not easy to physically separate the coating from the substrate (for example, by machining) without damaging it. In addition, even if the coating can be successfully separated from the substrate, it is not a simple matter to measure directly the thermal conductivity of the coating film, especially if it is very thin.

The laser flash (LF) method is commonly used to accurately measure the thermal diffusivity and specific heat capacity, and hence thermal conductivity, of materials [8]. For bulk materials, this technique has the advantage of being straightforward to perform, as sample preparation is simple and the measuring time is short [9–15]. However, the LF method is usually applied assuming the specimen to be uniformly dense and opaque. This is not the case for coatings deposited by EB-PVD, which normally have a highly non-uniform structure, thereby making the measurement of thermal conductivity in such materials non-trivial.

To solve this problem, in a previous paper [16] we proposed an equation for determining the thermal conductivity of coatings from double layer (coating and substrate) measurements using the response function method, which itself is based on the LF method. It has been reported that the response function method is a useful way to analyze one-dimensional heat diffusion across multi-layers materials [17]. In our previous work, we also reported the thermal conductivity of EB-PVD coatings deposited on zirconia substrates as a function of substrate thickness [16].

In this paper we report the thermal conductivity derived from heat diffusion results of ZrO_2–4 mol% Y_2O_3 (YSZ) coated samples as a function of coating thickness. For this purpose, YSZ coatings with various thicknesses were deposited on superalloy substrates by EB-PVD.

2. Experimental procedure

Disc-shaped substrates made from a nickel-based superalloy (Inconel 738, Mitsubishi Materials Co.) were machined to 10.0 mm diameter and 1.5 mm thickness. ZrO_2–4 mol% Y_2O_3 coatings were applied to the substrates by EB-PVD in the manner illustrated in Fig. 1(a). A bond coat was not used in this study to avoid introducing complicating effects that the different properties of the bond coat layer and extra interfaces would have on the thermal conductivity of the coated specimens.

To deposit the ceramic coatings, superalloy substrates were inserted into a custom-made holder assembly and placed under vacuum. The substrates were first preheated at 1000 °C in a heating chamber using graphite heating elements. The substrates were then moved to the coating chamber for deposition. An electron beam evaporation process was used to deposit the film at a rate of 5 μm/min under a vacuum of 10^{-4} Pa using a 45 kW electron gun and a substrate rotation speed of 5 rpm.

* Corresponding author. Tel.: +81 29 859 2453; fax: +81 29 859 2401.
E-mail address: JANG.Byungkoog@nims.go.jp (B.-K. Jang).

0925-8388/$ – see front matter © 2010 Elsevier B.V. All rights reserved.
doi:10.1016/j.jallcom.2010.08.162

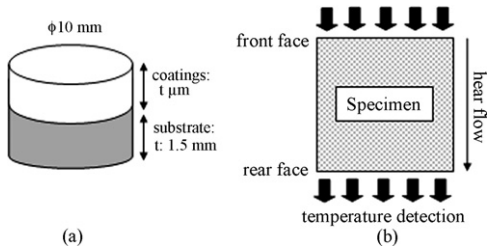

Fig. 1. Schematic diagram illustrating (a) sample preparation, and (b) heating by the laser pulse method.

Samples were prepared with coating thicknesses in the range of 68–754 μm. The density of each specimen was determined by measuring its mass with an electronic balance and its volume with a micrometer. Thermal diffusivity and specific heat capacity were determined at room temperature by the laser flash method [8,16] using a thermal analyzer (Kyoto Densi, LFA-501).

The laser flash method involves subjecting the entire front face of a specimen to a very short burst of energy from a laser and measuring the temperature rise on the other side (rear face) with an infrared detector, as shown schematically in Fig. 1(b). Prior to measuring the thermal diffusivity, the samples were sprayed with colloidal graphite to ensure complete and uniform absorption of the laser pulse and similar surface radiative characteristics for all samples.

The thermal conductivity of the specimens was then determined directly using

$$k = \alpha C \rho \quad (1)$$

where k is the thermal conductivity, α is the thermal diffusivity, C is the specific heat, and ρ is the density of the specimen. The microstructure of the coated specimens was analyzed by SEM.

3. Results and discussion

3.1. Microstructure of EB-PVD coatings

Typical microstructures of the EB-PVD coatings viewed perpendicular to their fracture surfaces are shown in Fig. 2. The fracture surfaces of the coatings clearly reveal a columnar microstructure with all the columnar grains oriented in the same direction, i.e., perpendicular to the substrate. Similarly textured microstructures were obtained by EB-PVD of zirconia on zirconia substrates [18]. The width of the columnar grains varies with the distance from the substrate even though the columns have the same crystallographic orientation throughout.

Table 1
Physical measurements of combined EB-PVD ZrO_2–4 mol% Y_2O_3 coating and substrate specimens.

Coating thickness (μm)	Density (g/cm^3)
68	8.12
89	8.06
103	7.98
164	7.87
264	7.63
371	7.40
569	7.09
754	6.98

At the beginning of the deposition process, nuclei form on the substrate with random orientations, as can be seen in Fig. 2(b), and grow to become grains that are better aligned as they extend upwards, away from the substrate (Fig. 2(d)). Consequently the grains are wider towards the top of the columns compared with near the coating–substrate interface, resulting in a tapered columnar structure. Gaps between the columnar grains can also be clearly observed, particularly towards the top of the coatings.

3.2. Thermal properties of double layers

Table 1 lists the experimentally determined densities of combined ZrO_2–4 mol% Y_2O_3 coating and substrate specimens. Fig. 3 shows the temperature rise response behavior at the rear surface as a function of time for combined coating and substrate (double layer) specimens. The time taken for the maximum temperature to be reached in the temperature rise curves increased with increasing coating thickness.

By solving the one-dimensional thermal conduction equation assuming the ideal conditions in Fig. 1(b), the following temperature response on the rear face of the specimen is obtained [8]:

$$\Delta T = \Delta T_{\mathrm{m}} \left[1 + 2 \sum_{i=1}^{\infty} (-1)^n \exp\left(\frac{-n^2 \pi^2}{L} \alpha t \right) \right] \quad (2)$$

where α and L are the thermal diffusivity and the thickness of the specimen, respectively; ΔT is the temperature rise of the speci-

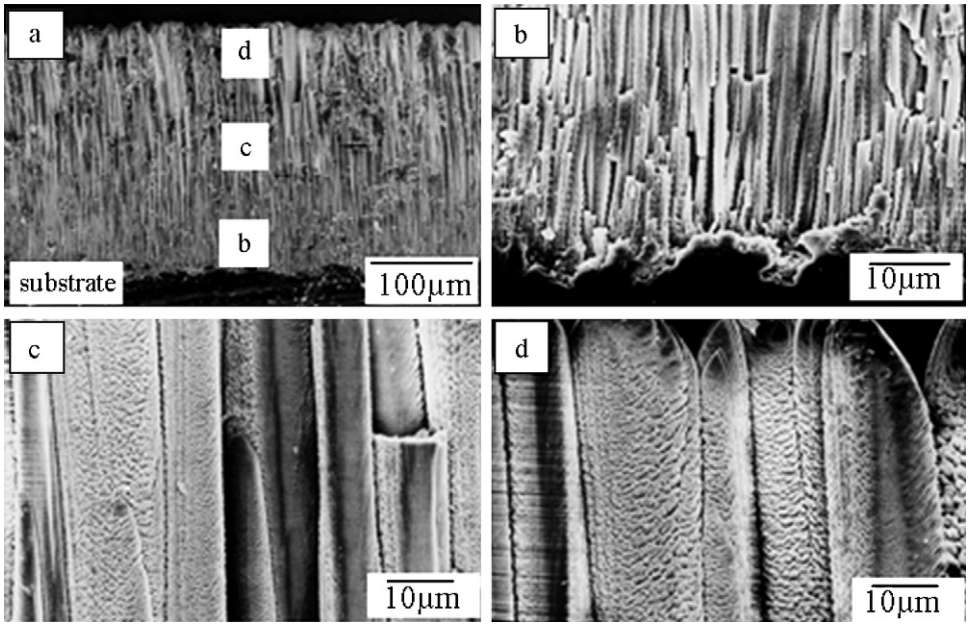

Fig. 2. SEM micrographs of (a) a cross-section of a 264 μm thick ZrO_2–4 mol% Y_2O_3 coating at low magnification, and (b–d) magnified views of the same coating at different distances from the substrate, as labeled in (a).

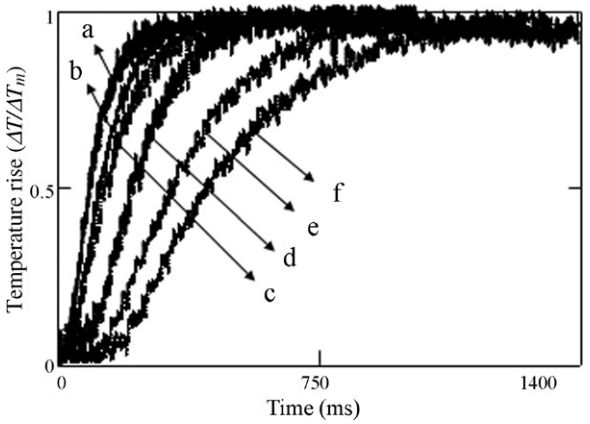

Fig. 3. Temperature rise curves as a function of time at the rear surfaces of specimens after laser pulse heating for combined ZrO_2–4 mol% Y_2O_3 coating and substrate specimens with coating thickness: (a) 68 μm, (b) 103 μm, (c) 264 μm, (d) 371 μm, (e) 569 μm, and (f) 754 μm (ΔT is the difference between temperature at time t and the minimum temperature; ΔTm is the difference between minimum and maximum temperatures).

men; ΔT_m is its maximum value; and t is the time after the pulse heating.

Fig. 4 shows the relationship between thermal conductivity, diffusivity and coating thickness for the combined coating and substrate specimens. The thermal diffusivity (α) is described by the following equation:

$$\alpha = \frac{1.38L^2}{\pi^2 t_{1/2}} \tag{3}$$

where L is the thickness of the specimen and $t_{1/2}$ is the time period corresponding to a temperature rise to half of the maximum temperature at the rear face of the specimen.

When calculating the thermal diffusivity using Eq. (3), the method of determining $t_{1/2}$ assumes that heat diffusion occurs across a uniform, pure and isotropic material. If this is the case, its value is reliable. However, the present specimens are non-uniform, consisting of a porous coating layer bonded to a dense substrate, and, similar to many other multi-layer materials, are thus not ideal for this kind of measurement. Consequently, the method of estimating heat diffusion in these double layer specimens must be reconsidered if the thermal conductivity of the coating layer is to be calculated accurately.

Baba et al. suggested that heat diffusion across a thin multi-layer material can be analyzed using the "response function method" [19,20]. For double layer materials, the area bounded by the temperature rise curve and the maximum temperature line at the rear face of the coated specimen after laser pulse heating, A, can be obtained by integration of the temperature rise response curve (Fig. 3). This area is called the "areal thermal diffusion time", and according to the response function method, if boundary thermal resistance is ignored, it can be expressed as:

$$A = \int_0^\infty [1 - b\sqrt{\tau}\cdot T_r(t)]\ \ dt = \lim_{\xi\to 0}\left[\frac{1}{\xi} - b\sqrt{\tau}\cdot \tilde{T}_r(\xi)\right] \tag{4}$$

where b and τ are thermal effusivity and heat diffusion time, respectively.

Fig. 5 shows the areal thermal diffusion time for the double layer specimens obtained by integration of the temperature rise curves in Fig. 3. This shows that the areal thermal diffusion time of the specimens increases with increasing coating thickness.

To derive the thermal conductivity of the coatings themselves, each double layer system can be modeled as two parallel layers, layer 1 and layer 2, as illustrated in Fig. 6. If heat flow ideally proceeds from layer 1 to layer 2, in Laplace space the four-fold matrices ($\tilde{S}_1(\xi)$) of layer 1 can be expressed as

$$\begin{bmatrix}\tilde{q}_2(\xi)\\ \tilde{T}_2(\xi)\end{bmatrix} = \tilde{S}_1(\xi)\cdot\begin{bmatrix}\tilde{q}_2(\xi)\\ \tilde{T}_2(\xi)\end{bmatrix} \tag{5}$$

where $\tilde{q}_1(\xi)$, $\tilde{q}_3(\xi)$ and $\tilde{q}_2(\xi)$ are heat fluxes at layer 1, layer 2 and the interface, respectively, and $\tilde{T}_1(\xi)$, $\tilde{T}_3(\xi)$ and $\tilde{T}_2(\xi)$ are the instantaneous temperatures at layer 1, layer 2 and the interface, respectively. Each component can be written as follows:

$$\tilde{q}_2(\xi) = \cosh(\sqrt{\xi\tau_1})\cdot\tilde{q}_1(\xi_1) - b_1(\xi)\cdot\sinh(\sqrt{\xi\tau_1})\cdot\tilde{T}_1(\xi) \tag{6}$$

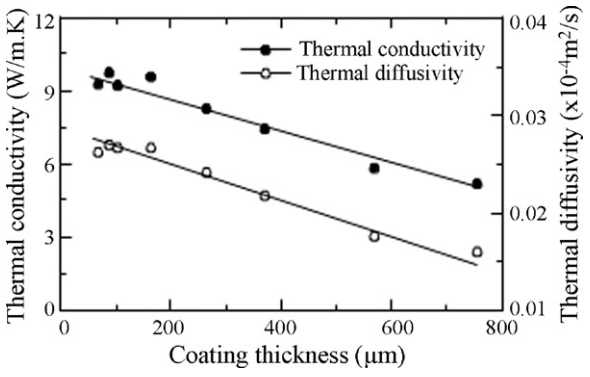

Fig. 4. Thermal conductivity and thermal diffusivity as a function of coating thickness for combined ZrO_2–4 mol% Y_2O_3 coating and substrate specimens.

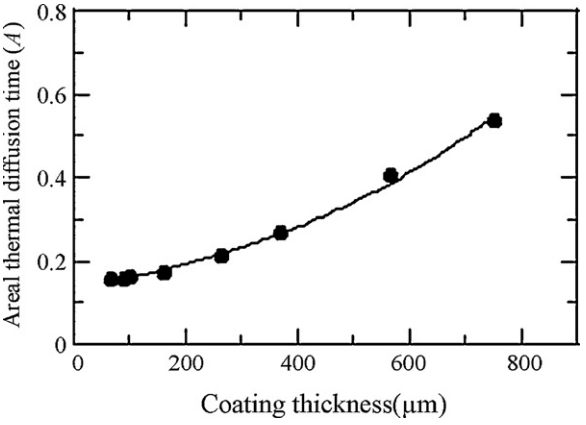

Fig. 5. Areal thermal diffusion time values as a function of ZrO_2–4 mol% Y_2O_3 coating thickness for combined coating and substrate specimens.

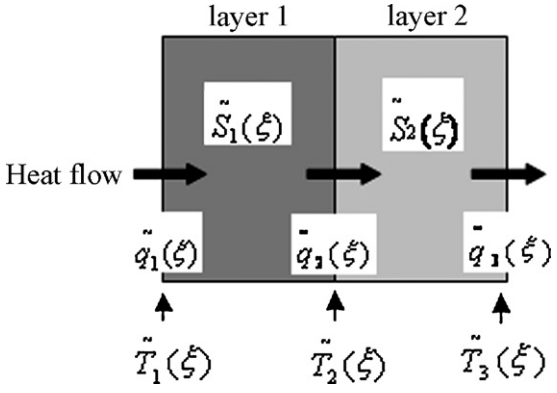

Fig. 6. Schematic diagram of four-pole matrices to explain heat diffusion across double layer materials.

$$\tilde{T}_2(\xi) = -\frac{1}{b_1(\xi)} \cdot \sinh(\sqrt{\xi\tau_1}) \cdot \tilde{q}_1(\xi_1) + \cosh(\sqrt{\xi\tau_1}) \cdot \tilde{T}_1(\xi) \quad (7)$$

The same four-fold matrix ($\tilde{S}_2(\xi)$) method can be adopted for layer 2, giving the following equation:

$$\begin{bmatrix} \tilde{q}_2(\xi) \\ \tilde{T}_2(\xi) \end{bmatrix} = \tilde{S}_2(\xi)^{-1} \cdot \begin{bmatrix} \tilde{q}_3(\xi) \\ \tilde{T}_3(\xi) \end{bmatrix} \quad (8)$$

$$\tilde{q}_2(\xi) = \cosh(\sqrt{\xi\tau_2}) \cdot \tilde{q}_3(\xi) + b_2(\xi) \cdot \sinh(\sqrt{\xi\tau_2}) \cdot \tilde{T}_3(\xi) \quad (9)$$

$$\tilde{T}_2(\xi) = \frac{1}{b_2(\xi)} \cdot \sinh(\sqrt{\xi\tau_2}) \cdot \tilde{q}_3(\xi) + \cosh(\sqrt{\xi\tau_2}) \cdot \tilde{T}_3(\xi) \quad (10)$$

By substituting the terms $\tilde{q}_1(\xi) = 1$ and $\tilde{q}_3(\xi) = 0$ into Eqs. (6), (7), (9) and (10), $\tilde{T}_3(\xi)$ can be obtained from

$$\tilde{T}_3(\xi) = \frac{1}{\sqrt{\xi}} \cdot \frac{1}{\left[b_1 \sinh(\sqrt{\xi\tau_1})\cosh(\sqrt{\xi\tau_2}) + b_2 \cosh(\sqrt{\xi\tau_1})\sinh(\sqrt{\xi\tau_2})\right]} \quad (11)$$

Here, by substituting $\tilde{T}_r(\xi) = \tilde{T}_3(\xi)$, Eq. (4) can be rewritten as:

$$A = \lim_{\xi \to 0} \left[\frac{1}{\xi} - (b_1 \cdot \sqrt{\tau_1} + b_2 \cdot \sqrt{\tau_2}) \cdot \tilde{T}_3(\xi)\right] = \frac{b_1\tau_1^{3/2} + 3b_2\tau_1\tau_2^{1/2} + 3b_1\tau_1^{1/2}\tau_2 + b_2\tau_2^{3/2}}{6 \cdot (b_1\sqrt{\tau_1} + b_2\sqrt{\tau_2})} \quad (12)$$

where subscripts 1 and 2 correspond to layers 1 and 2, respectively. By rearrangement of Eq. (12), the thermal conductivity (k_2) of layer 2 is given by for double layer specimen [16]:

$$k_2 = \frac{d_2^2 C_2 \rho_2 (3d_1 C_1 \rho_1 + d_2 C_2 \rho_2)}{6A(d_1 C_1 \rho_1 + d_2 C_2 \rho_2) - d_1^2 C_1 \rho_1 (d_1 C_1 \rho_1 + 3d_2 C_2 \rho_2)/k_1} \quad (13)$$

where d_1, C_1, ρ_1 and d_2, C_2, ρ_2 correspond to the thicknesses, specific heats and densities of layers 1 and 2, respectively, and k_1 is the thermal conductivity of layer 1. In the present work, layer 1 and layer 2 correspond to substrate and coating, respectively. A more detailed account of the procedure used to derive Eq. (13) from Eq. (12) is given in Ref. [16].

3.3. Thermal conductivity of coatings

The measured density and specific heat used in Eq. (13) are 8.17 g/cm^3 and 0.440 kJ/(kg·K) for the substrate, and 4.91 g/cm^3 and 0.448 kJ/(kg·K) for the coatings, respectively to calculate the thermal conductivities of the coatings. The thermal conductivity of the substrate alone was 9.43 W/(mK).

Fig. 7 shows the calculated thermal conductivities from Eq. (13) as a function of coating thickness, and compares them with direct thermal conductivity measurements of the coating layers. These thermal conductivity values for the coating layers were derived according to Eq. (1) after first separating the coating from the substrate by diamond wheel machining.

The calculated thermal conductivities of the coatings tend to increase with increasing coating thickness. As seen in Fig. 7, the calculated thermal conductivities are in good agreement with the directly measured thermal conductivities of the coatings. However, it was not possible to measure directly the thermal conductivities of individual coatings thinner than 200 μm because they are too fragile to be handled during LF measurements. It can thus be seen that Eq. (13) is a useful means of determining the thermal conductivity of coating layers without the need to separate the coating from the substrate, particularly in the case of thin film coatings.

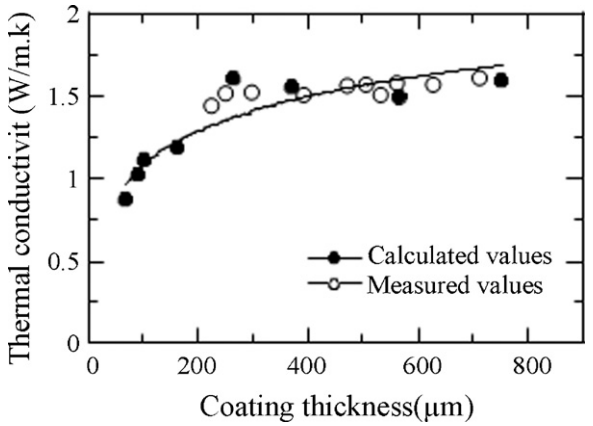

Fig. 7. Thermal conductivity as a function of coating thickness for ZrO_2–4 mol% Y_2O_3 coatings deposited by EB-PVD. Values were obtained directly by separating coatings from substrate (measured) or extracted from double layer measurements using Eq. (13) (calculated).

The thermal conductivities of the coatings measured in this study are low compared to the value of 2.59 W/(m K) reported for sintered bodies of ZrO_2–4 mol% Y_2O_3 [16]. Furthermore, coating layers thinner than 200 μm have considerably lower thermal conductivities than thicker specimens (i.e., with thicknesses >200 μm). Thermal conductivity can thus be seen to strongly depend on the microstructure of the materials.

This conclusion is borne out by the results of microstructural analysis. Fig. 8 shows the number of column boundaries per unit area for each ZrO_2–4 mol% Y_2O_3 coating deposited by EB-PVD. From this it can be seen that the number of boundaries decreases with increasing coating thickness. Typical SEM images of thin and thick ZrO_2–4 mol% Y_2O_3 coatings deposited by EB-PVD are shown in Fig. 9. In Fig. 9(a) it can be seen that the width and size of the columns in the thinner coating layer are considerably smaller than in the thicker coating, resulting in many columns per unit area. In contrast, the columns in the thicker coating (Fig. 9(b)) are much larger and coarser.

Lower thermal conductivity generally occurs because of phonon scattering in the lattice, since the contribution of phonon (lattice vibrations) on thermal conductivity is given by [21–23]:

$$k = \frac{1}{3} \int C\rho v l \quad (14)$$

where C is the specific heat, ρ is density, v is the speed of sound and l is the phonon mean free path. From Eq. (14), it can be seen that if

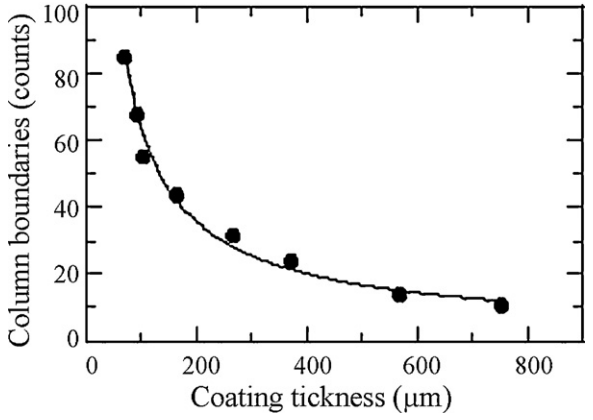

Fig. 8. Density of column boundaries (per 100 μm width) as a function of coating thickness for ZrO_2–4 mol% Y_2O_3 coatings.

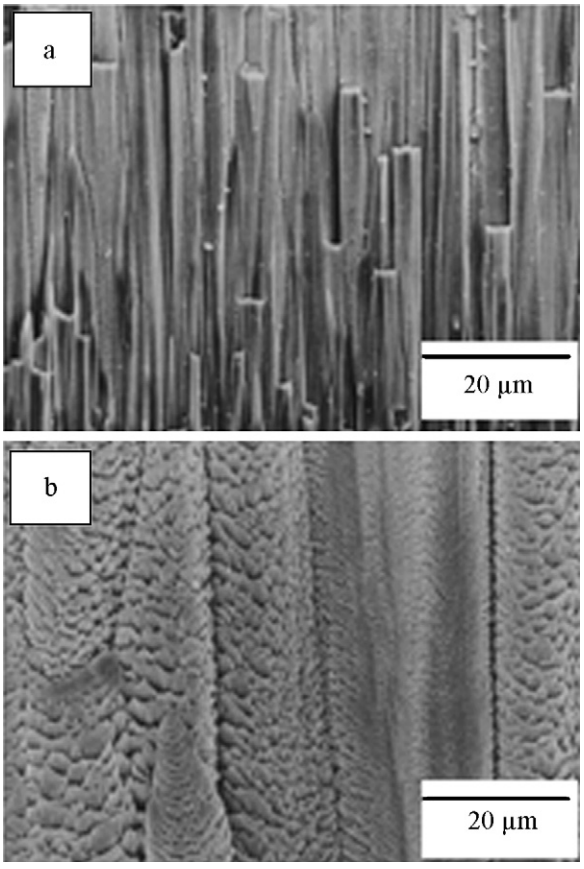

Fig. 9. SEM micrographs of cross-sections of ZrO_2–4 mol% Y_2O_3 coatings deposited by EB-PVD for coating thicknesses of: (a) 103 μm and (b) 754 μm.

the phonon mean free path is decreased, thermal conductivity will also decrease.

Scattering occurs because phonons interact with imperfections such as dislocations, vacancies, pores and grain boundaries, and the greater the density of these, the greater the scattering. The phonon mean free path (l_p) of a lattice phonon is defined by [24,25]:

$$\frac{1}{l_p} = \frac{1}{l_i} + \frac{1}{l_{gb}} + \frac{1}{l_{vac}} + \frac{1}{l_{strain}} \quad (15)$$

where l_i, l_{gb}, l_{vac} and l_{strain} are the contributions due to interstitials, grain boundaries, vacancies and lattice strain, respectively. The grain boundary density of a material thus affects the phonon mean free path, and hence the degree of phonon scattering. In terms of microstructural properties, the column boundaries in our layered materials act similar to grain boundaries in bulk, sintered materials. A higher concentration of column boundaries therefore also contributes to a decreased phonon mean free path.

Our measurements show that the increased density of column boundaries in coatings thinner than 200 μm significantly reduces the phonon mean free path, and hence thermal conductivity. These results are therefore consistent with earlier studies of the effects of grains, column size and coating thickness on thermal conductivity of CVD or PVD coatings [21,22] and EB-PVD [26], which showed that the thermal conductivity of coatings decreases with increasing grain boundary density as well as columnar porosity.

4. Conclusions

A series of ZrO_2–4 mol% Y_2O_3 coatings with thicknesses in the range of 68–754 μm were deposited on superalloy substrates by EB-PVD. Fracture surfaces of the coatings revealed a porous columnar microstructure with gaps between columnar grains.

Thermal diffusivities of combined coating and substrate (double layer) specimens were measured using the laser flash method. The thermal conductivities of the coatings were successfully derived from these using the response function method. The values obtained were in good agreement with the thermal conductivities measured directly from coatings separated from the substrates by diamond wheel machining, thus demonstrating the accuracy and reliability of the double layer method, as well as its usefulness for calculating thermal conductivities of coatings in cases where the coating is too thin or fragile to be removed from the substrate.

The thermal conductivity of zirconia coatings increased with increasing coating thickness. Coatings thinner than 200 μm contained a higher density of column boundaries than thicker coatings. A higher density of column boundaries led to significantly reduced thermal conductivities in the coating as a result of the reduction in phonon mean free path and increased phonon scattering that these boundaries cause.

Acknowledgments

The work was carried out with financial support from NEDO and the Korea Institute of Ceramic Engineering and Technology (KIER). First author is very grateful to Dr. C.A.J. Fisher of JFCC for useful discussions and critical reading of the manuscript.

References

[1] H.J.R. Scheibe, U. Schulz, Surf. Coat. Technol. 201 (2007) 7880.
[2] U. Schulz, B. Saruhan, K. Fritscher, C. Leyens, Int. J. Appl. Ceram. Technol. 1 (2004) 302.
[3] C. Leyens, U. Schulz, K. Fritscher, M. Bartsh, M. Peter, W.A. Kaysser, Z. Metallkund. 92 (2001) 762.
[4] C.G. Levi, Curr. Opin. Solid State Mater. Sci. 8 (2004) 77.
[5] J. Singh, D.E. Wolfe, J. Singh, J. Mater. Sci. 37 (2002) 3261.
[6] D.M. Zhu, R.A. Miller, Surf. Coat. Technol. 108–109 (1998) 114.
[7] O. Unal, T.E. Mitchell, A.H. Heuer, J. Am. Ceram. Soc. 77 (1994) 984.
[8] W.J. Parker, R.J. Jenkins, C.P. Butler, G.L. Abbott, J. Appl. Phys. 32 (1961) 1679.
[9] B.K. Jang, H. Matsubara, Scripta Mater. 52 (2005) 553.
[10] A.F. Renteria, B. Saruhan, U. Schulz, H.J.R. Scheibe, J. Haug, A. Wiedenmann, Surf. Coat. Technol. 201 (2006) 2611.
[11] J.F. Bisson, D. Fournier, M. Poulain, O. Lavigne, R. Mévrel, J. Am. Ceram. Soc. 83 (2000) 1993.
[12] H. Wang, R.B. Dinwiddie, J. Therm. Spray Technol. 9 (2000) 210.
[13] H.B. Guo, H. Xu, X.F. Bi, S. Gong, Mater. Sci. Eng. A 325 (2002) 389.
[14] A. Azzopardi, R. Mévrel, B.S. Ramond, E. Olson, K. Stiller, Surf. Coat. Technol. 177–178 (2004) 131.
[15] E. Reinhold, P. Botzler, C. Deus, Surf. Coat. Technol. 120–121 (1999) 77.
[16] B.K. Jang, M. Yoshiya, N. Yamaguchi, H. Matsubara, J. Mater. Sci. 39 (2004) 1823.
[17] T. Baba, N. Taketoshi, Proc. 21th Jpn. Symp. Thermophys. Prop. Tokyo (2000) 229.
[18] B.K. Jang, H. Matsubara, Surf. Coat. Technol. 200 (2006) 4594.
[19] T. Baba, Jpn. J. Thermophys. Prop. 7 (1993) 14.
[20] T. Baba, N. Taketoshi, 21st Jpn. Symp. Thermophys. Prop. (2000) 229.
[21] P. Debye, Vortrageüber die Kinetishe Theorie, Tuelner B.G., Leipsig, 1914.
[22] P.G. Klemens, Thermal Conductivity of Solids, Academic Press, London, 1969.
[23] B.K. Jang, Y. Sakka, Sci. Technol. Adv. Mater. 8 (2007) 655.
[24] K.J. Lawson, J.R. Nicholl, D.S. Rickerby, Adv. Surf. Eng. 1 (1997) 83.
[25] J.R. Nicholl, K.J. Lawson, A. Johnstone, D.S. Rickerby, Mater. Sci. Forum. 369–372 (2001) 595.
[26] H.J.R. Scheibe, U. Schulz, T. Krell, Surf. Coat. Technol. 200 (2006) 5636.